TRIUMF

Document: 114221

Design Note TRI-DN-14-16

Optics design for a high-field (2kG) BNQR Spectrometer

Document Type: **Design Note**

Release: **2** **Release Date** **2015-05-12**

Author(s): **S. Saminathan, R. Baartman**

	Name:	Review Scope	Signature:	Date:
Author:	S. Saminathan		APPROVED	2015/04/10
	R. Baartman			" " "
Reviewed:	F. Ames		APPROVED	2015/05/04
Reviewed:	G. Morris			2015/4/28
Reviewed:	R. Kiefl		APPROVED	2015/5/01
Approved:	L. Merminga			2015/5/08

History of Changes

Release Number	Date	Description of Changes	Author(s)
1	12-11-2014	Initial Release (unsigned)	S. Saminathan
2	12-05-2015	Reviewed Design Note	S. Saminathan R. Baartman

Contents

1 Abstract

A new β-NQR beamline is proposed for superconducting RF material studies. In this design note the beam optics design, beamline layout and the optical elements specifications for the transport of low energy radio-active ion beams through the proposed β-NQR spectrometer are presented.

2 Introduction

2.1 Objective

The objective of this work is to design and install a high-field extension of the β-NQR spectrometer, up to 2000 G, along with a second access port onto the existing β-NQR platform.

2.2 Definitions

- **Coordinate system:** Right-handed cartesian coordinate system is used. The origin of the beam line is at the effective field boundary (EFB) of electrostatic bender (see Fig. 1). The initial beam parameters are defined at the location of 0.533 m from the EFB, which is also the location of beam waist.
- **Sample-1:** The mounting location of the first sample, which is located at 1.304 m from the origin (see Fig. 1). At this location the maximum background magnetic field is $\approx$ 220 G.
- **Sample-2:** The mounting location of the second sample, which is located at 2.314 m from the origin (see Fig. 1). At this location the maximum background magnetic field is $\approx$ 2000 G.
- **Decelerator:** A set of electrodes used to change the beam energy according to experiment requirements and also used as a electrostatic steerer by segmenting the electrodes into four quadrant (see Fig. 4).

2.3 Abbreviations

- **β-NMR:** Beta-detected nuclear magnetic resonances.
- **β-NQR:** Beta-detected nuclear quadrupole resonances.
- **SRF:** Superconducting radio-frequency.
- **UHV:** Ultra high vacuum.
- **EQ:** Electrostatic quadrupole.

- **EFB:** Effective field boundary.
- **FC:** Faraday cup.
- **COL:** Collimator.

3 Requirements

The β-NQR spectrometer is a unique method for probing electronic and magnetic properties of materials using a beam of hyper-polarized 8Li$^+$ [1]. Here the spin and external magnetic field are parallel to the sample face. This arrangement is ideal for measuring the depth dependence of magnetic field in the Meissner state of superconductors, which is the focus of superconducting rado-frequency (SRF) cavity studies. In order to investigate the properties of material (sample) as a function of depth in nano-metre (nm) scale the required magnetic rigidity of the particle is in the range between 0.0129 T m – 0.0705 T m. The external magnetic field transverse to the beam is presently limited to 220 G at sample-1 (see Fig. 1), whereas fields up to 2000 G at sample-2 are needed for SRF studies (proposed beamline) [2]. The pumped 3He cryostat is also very unique and will allow measurements down to 300 mK.

The proposed experimental facility is an upgrade of the existing beamline with an extension of ≈ 1 m beamline length. Each spectrometer is independently equipped with a helium cryostat and both are mounted on a high voltage platform which is electrically isolated from ground. The ion beam energy, and thus the depth of ion implantation, is controlled by adjusting the platform bias voltage.

The objective of this work is to build and install a high-field extension of the β-NQR spectrometer, up to 2000 G, along with a second access port onto the existing platform. The beam optics requirement is to deliver axially symmetric beam on the sample. The basic beam requirements are summarized in Table 1.

3.1 Constraints

- The beamline layout should fit within the existing cryostat platform.
- Optical components and the diagnostics devices should be UHV compatible.
- Wherever possible, the existing vacuum chamber, the electrostatic steerer and the diagnostic devices should be reused.
- Beamline layout should accommodate a thermal heat shield between the sample-2 and the rest of the beamline [i.e. to minimize any heat load on the sample-2 due to thermal radiation].

Beam	$8Li^+$
Beam energy on the sample-1	1 keV–30 keV
Beam energy on the sample-2	1 keV–30 keV
Typical beam energy on the sample-1 & 2	4 keV
Maximum magnetic field at sample-1	220 G
Maximum magnetic field at sample-2	2000 G
Beam position	Axially centered
Half width of the beam size (2 rms)	0.002 m

Table 1: Basic beam requirements.

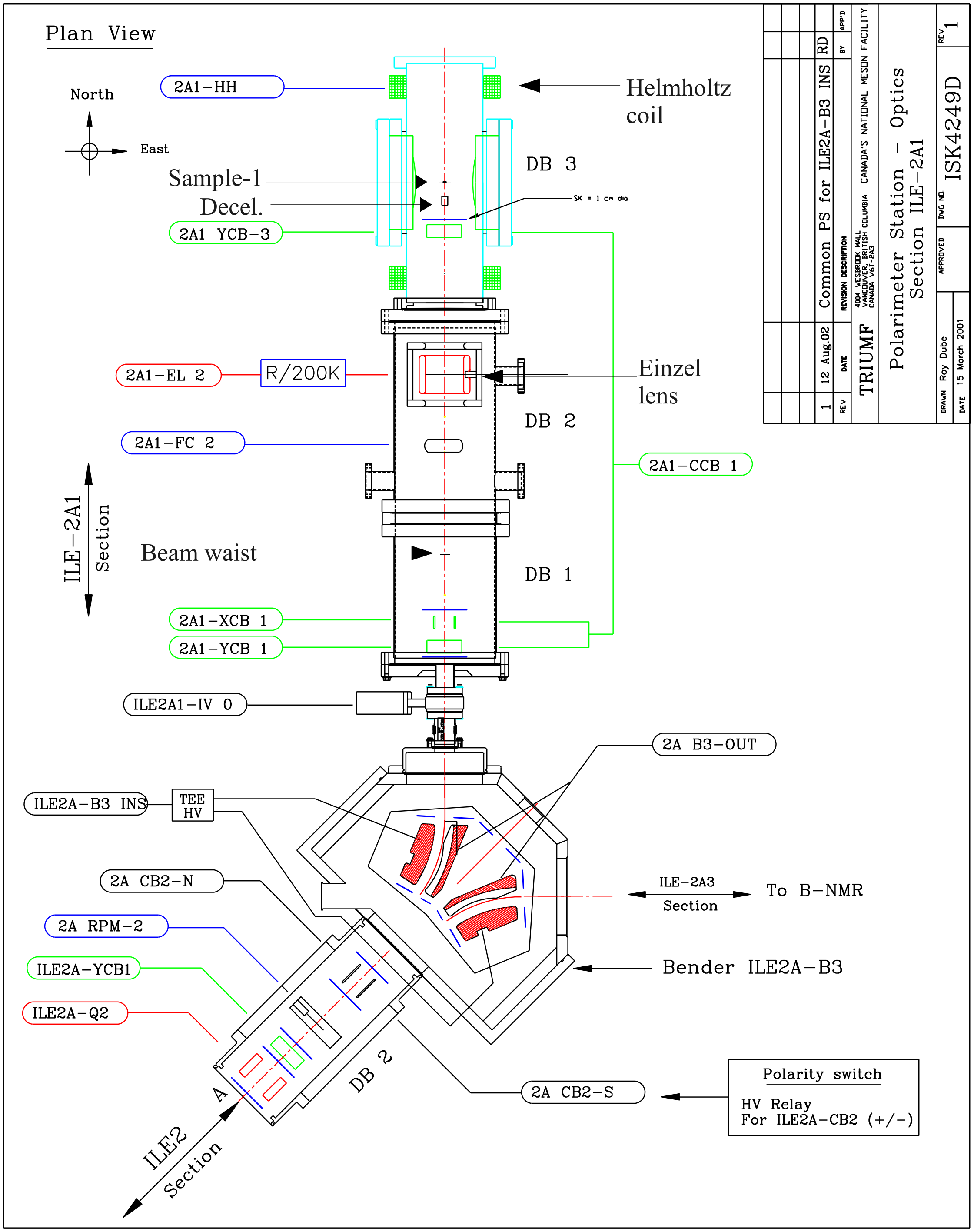

Figure 1: Layout of existing β-NQR beamline for maximum magnetic field around 240 G at the sample.

4 Existing β-NQR beamline

The β-NQR beamline consists of an Einzel lens, Helmholtz magnet, decelerator, two vertical and a horizontal steerer (see the beamline layout shown in Fig. 1). Sample-1 is located at the end of the beamline at the center of the Helmholtz coil (ILE2A1-HH) and it is capable to produce field up to 240 G only. The Einzel lens (ILE2A1-EL2) focus the beam on the sample-1 and the required beam energy on the sample-1 is controlled by the decelerator by adjusting its potential. Geometry of the decelerator and its schematic layout are shown in Fig. 2 & 3.

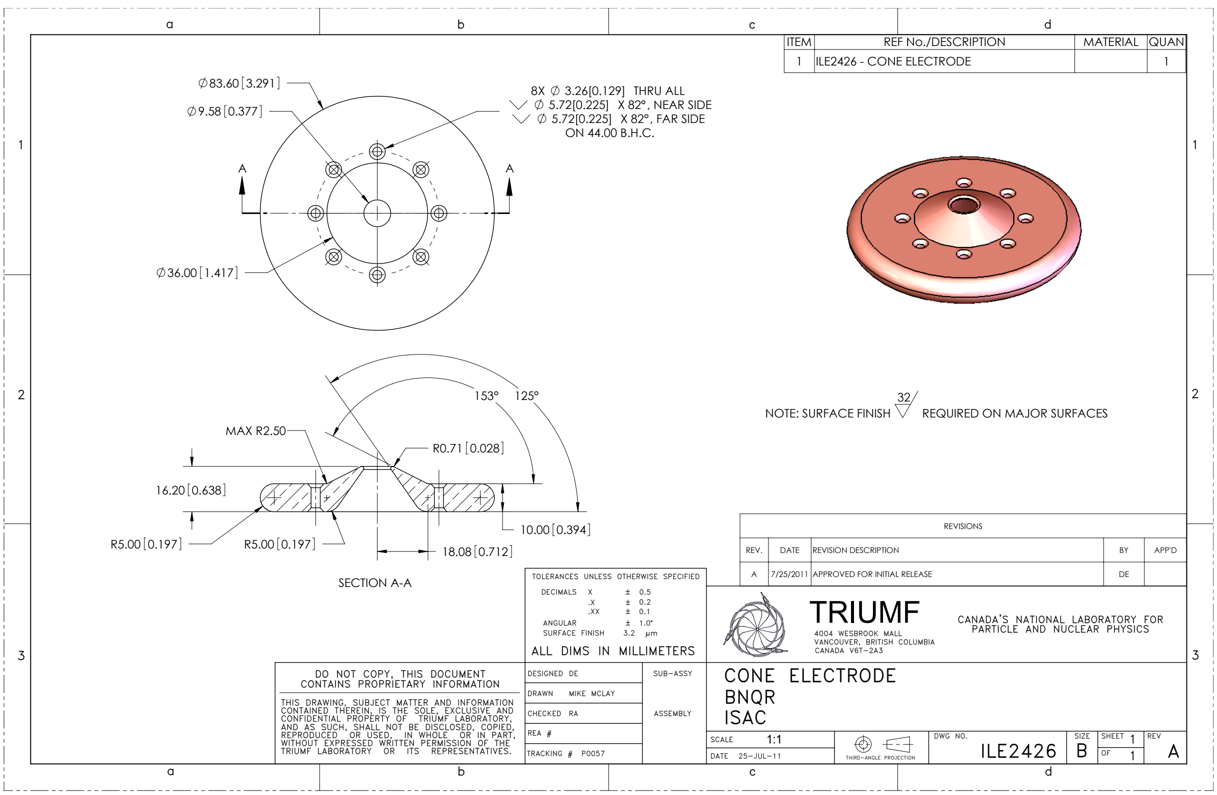

Figure 2: Geometry of the existing β-NQR decelerator.

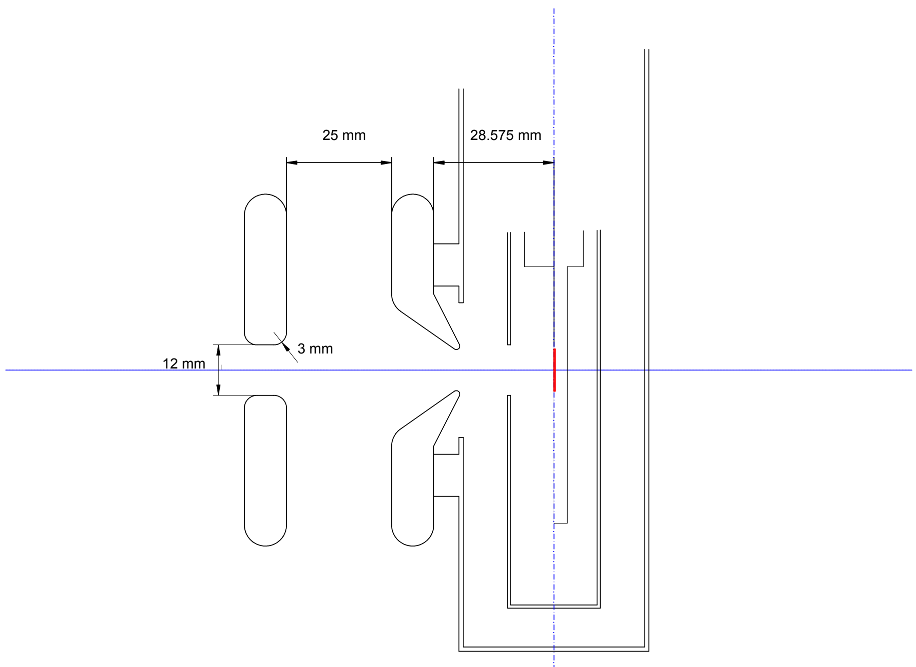

Figure 3: Layout of the existing β-NQR decelerator system.

5 Optics calculations for beamline upgrade

5.1 Electric/Magnetic modeling

The basic beam requirements for the proposed β-NQR beam facility are shown in Table 1. In the existing beamline the transverse deflection due to the Helmholtz field is mainly compensated by an electrostatic steerer (ILE2A1-YCB3) [7]. This alone is not sufficient at 2000 G field because the required compensation strength is quite strong. In the proposed beamline the decelerator is the primary compensating steerer for the deflection due to Helmholtz field in addition to the function of deceleration. Thus the existing geometry (see Fig. 2) will be replaced with a newly designed decelerator system (see Fig. 4). The proposed decelerator is segmented into four electrodes (see Fig. 4 & 5). It closely resembles the PSI design [6] to provide an electrostatic steering (see Fig. 8 & 9).

The electric/magnetic field calculations for the optical elements are done by using the code OPERA3D. The calculated potential along the axis of the decelerator is shown in Fig. 10. Cross-section view of the decelerator with Helmholtz magnet is shown in Fig. 6 and the dimension of the Helmholtz magnet is shown in Fig. 7. The calculated horizontal magnetic field component (B_x) along the axis of the Helmholtz magnet is given in Fig. 17.

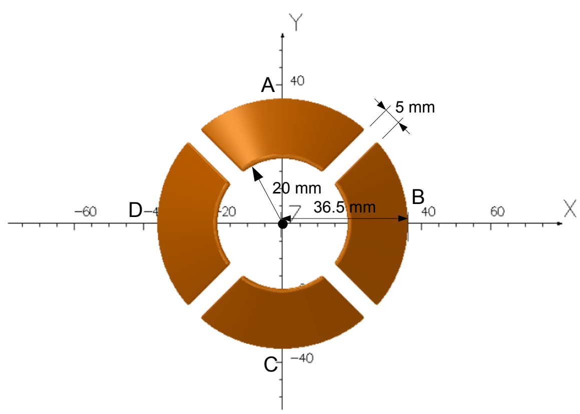

Figure 4: Geometry of the new segmented high-voltage electrodes with labels. X is the horizontal axis, Y is the vertical axis and Z is the beam axis points forward.

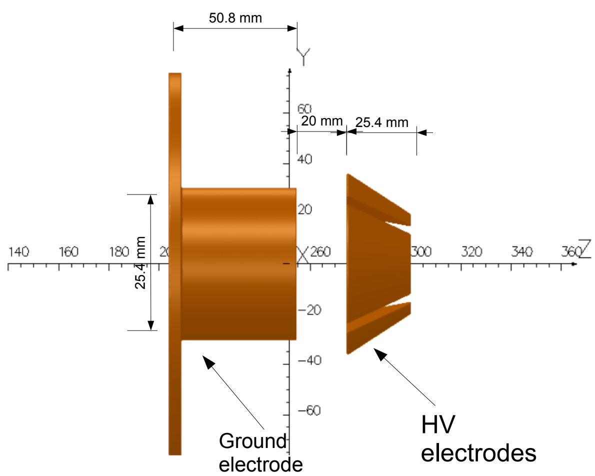

Figure 5: Geometry of the new decelerator.

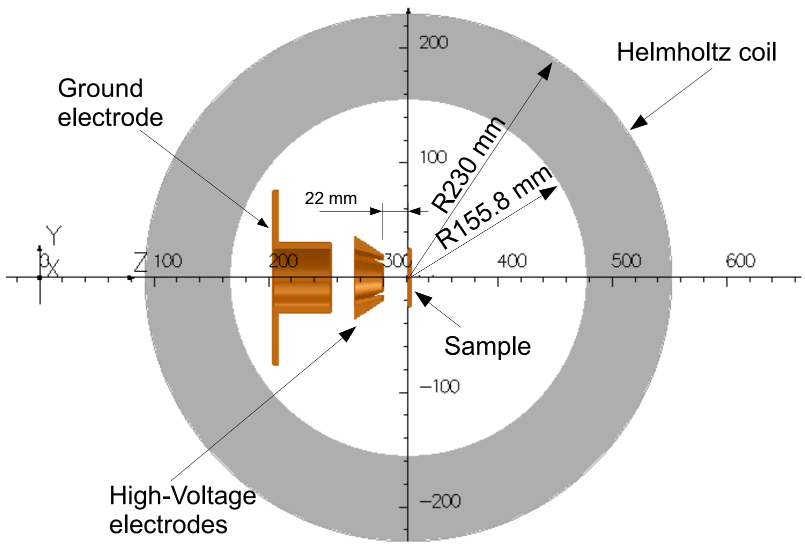

Figure 6: Cross section view of 2000 G Helmholtz coil (Grey) with a segmented decelerator (Brown) and sample (Brown). Beam is in Z-direction.

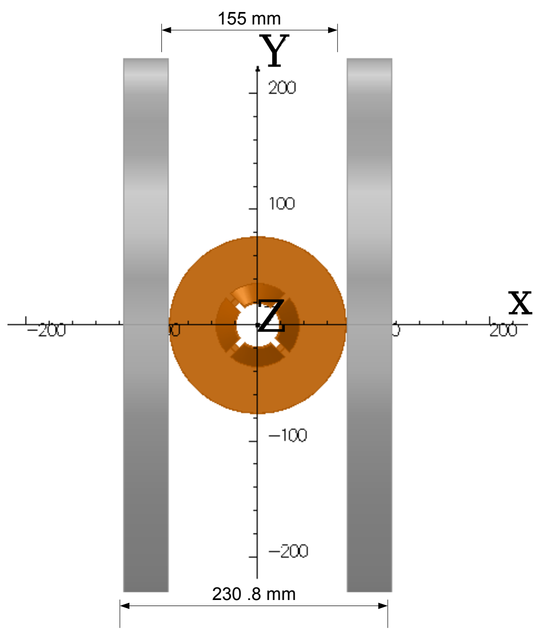

Figure 7: Helmholtz coil (Grey) with the segmented decelerator (Brown). Beam travels into the page.

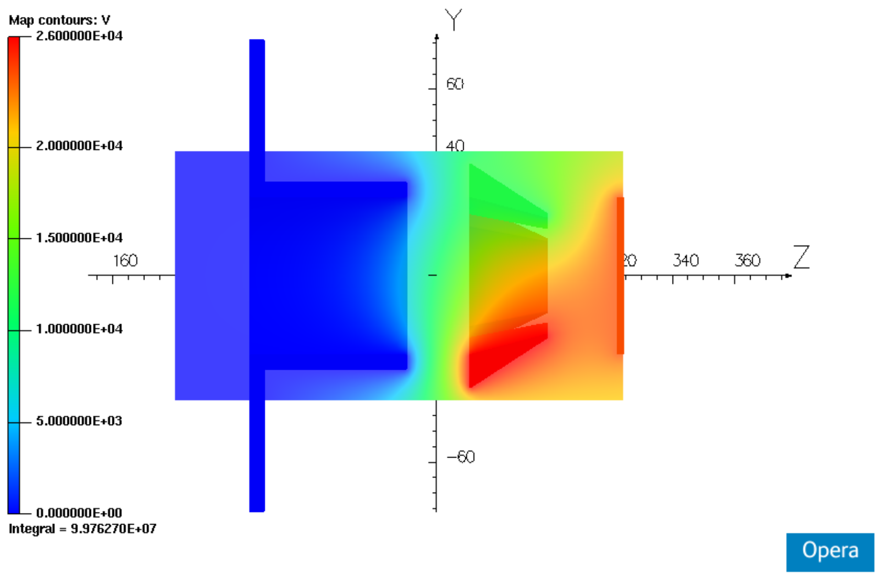

Figure 8: Calculated potential contour in the ZY plane for a typical applied potential of 12 kV (A), 24 kV (B & D) and 26 kV (C) to the decelerator electrodes. Labels A, B, C, D are defined in Fig. 4.

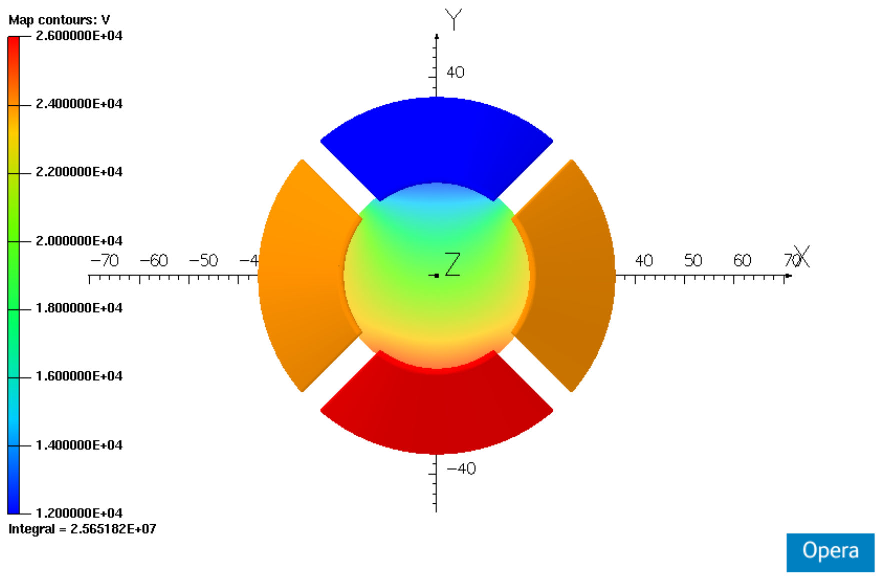

Figure 9: Calculated potential contour in the XY plane (at the decelerator exit, z = 0.3 m) for a typical applied potential of 12 kV (A), 24 kV (B & D) and 26 kV (C) to the decelerator electrodes. Labels A, B, C, D are defined in Fig. 4.

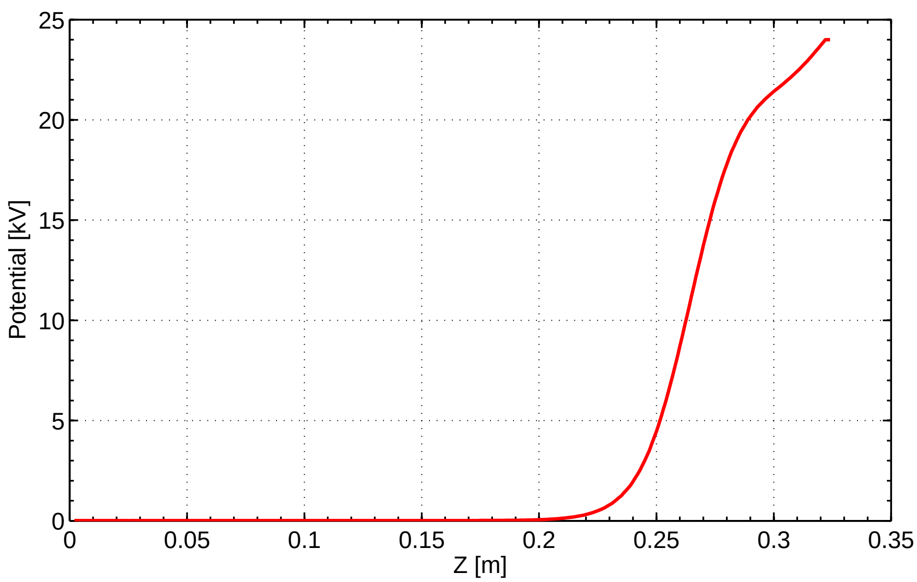

Figure 10: Calculated potential along the axis of the decelerator for a typical applied potential of 12 kV (A), 24 kV (B & D) and 26 kV (C) to the decelerator electrodes. Sample-2 is located at z = 0.322 m.

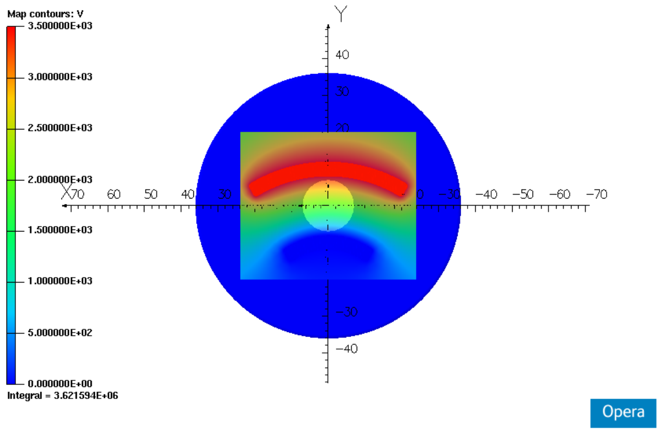

Figure 11: Calculated potential contour in the XY plane for a typical applied potential of 3.5 kV (Top) and 0 kV (Bottom) to the steerer electrodes [YCB4]. Z is the beam direction and beam travels into the page.

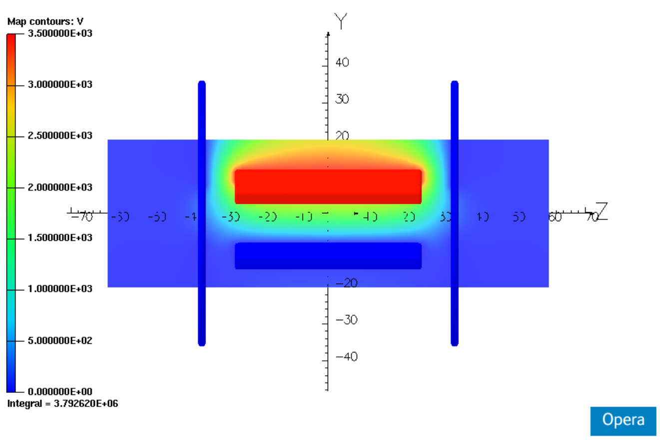

Figure 12: Calculated potential contour in the ZY plane for a typical applied potential of 3.5 kV (Top) and 0 kV (Bottom) to the steerer electrodes [YCB4].

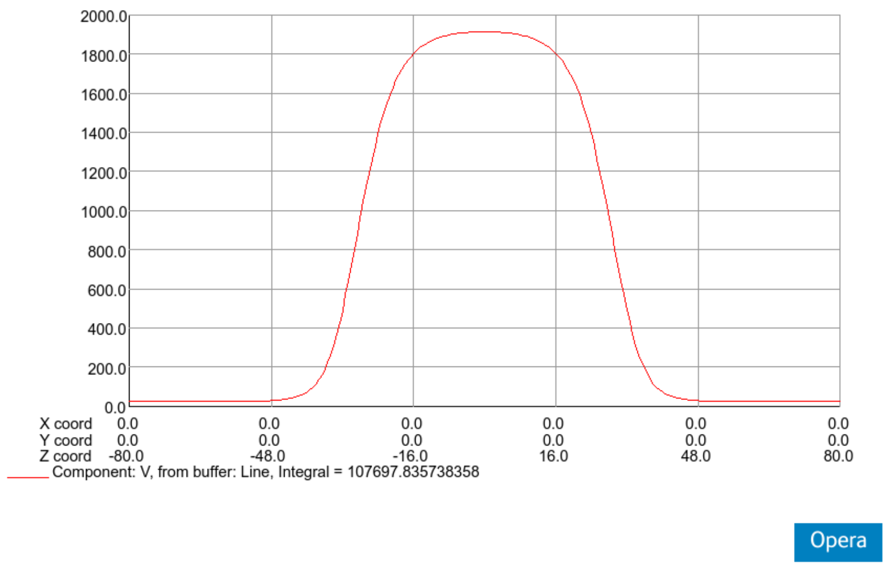

Figure 13: Calculated potential along the axis of the steerer for a typical applied potential of 3.5 kV (Top) and 0 kV (Bottom) to the steerer electrodes [YCB4].

5.2 Initial beam paramters

The phase-space distribution and the beam emittance ($\varepsilon = 12\ \mu$m [5]) are obtained from the envelope calculation performed for the beam transport downstream to the polarizer (see Fig. 14). The waist of the transported beam through the bender (ILE2A-B3) is formed at 0.53 m downstream to the EFB of the bender (ILE2A-B3). See Fig. 14 for the calculated beam envelope from the polarizer to the β-NQR beamline using the code TRANSOPTR. The basic beam parameters used in the beam transport calculation are shown in Table 2. The initial phase-space distribution (at the location of beam waist) used in this simulation is shown in Fig. 15.

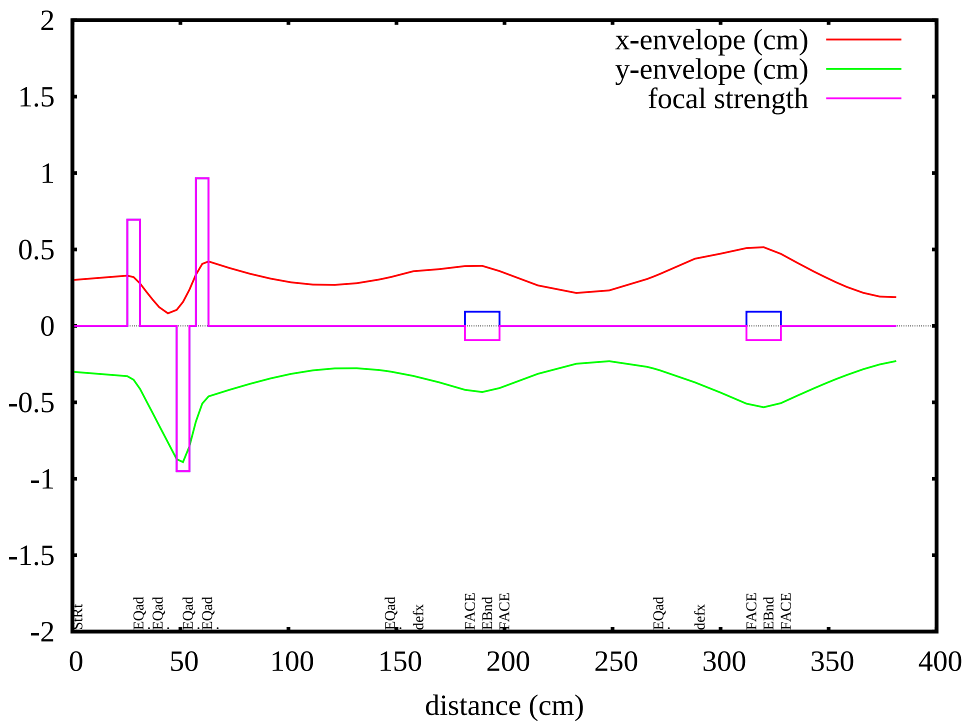

Figure 14: Calculated beam enevelope (2 rms) of the transported ion beam from the polarizer to downstream of the electrostatic bender (ILE2A-B3).

Beam	$8Li^+$
Initial beam energy	28 keV
Energy spread (2 rms)	2 eV
Horizontal half width of the beam [2 rms] (X)	2.0 mm
Horizontal half width of the beam divergence [2 rms] (X_p)	6.0 mrad
Vertical half width of the beam [2 rms] (Y)	2.0 mm
Vertical half width of the beam divergence [2 rms] (Y_p)	6.0 mrad
Emittance [4 rms] (ε)	12.0 μm

Table 2: Initial beam parameters at the location of beam waist (see Fig. 1) for the simulation of ion beam transport through the proposed β-NQR beamline.

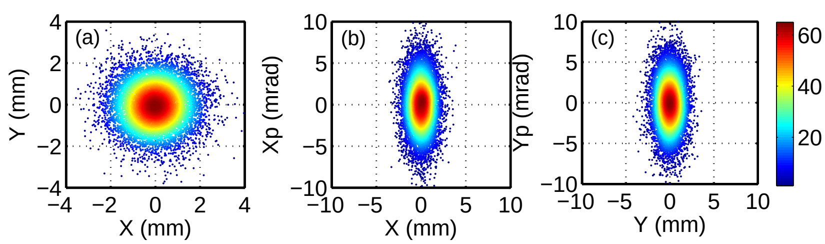

Figure 15: Simulated initial phase-space distributions of 28 keV 8Li$^+$ beam at the location of beam waist (see Fig. 1). Spatial profile (a), horizontal (b) and vertical (c) phase planes.

5.3 Beam Envelope

In the proposed beamline design the Einzel lens (see Fig. 1) will be replaced by an electrostatic quadrupole triplet to obtain a focusing on sample-1. In addition, a 1.02 m extension to the existing beamline will be constructed with a second focus (sample-2) located at the center of a 2000 G Helmholtz coil, and a second quadrupole triplet to obtain focusing on the sample-2. The length of the proposed beamline is defined by the existing infrastructure (e.g. cryostat, platform, etc.). A schematic layout of the beamline for 220 G field at sample-1 and the proposed beamline extension for 2000 G field at sample-2 are shown in Fig. 16.

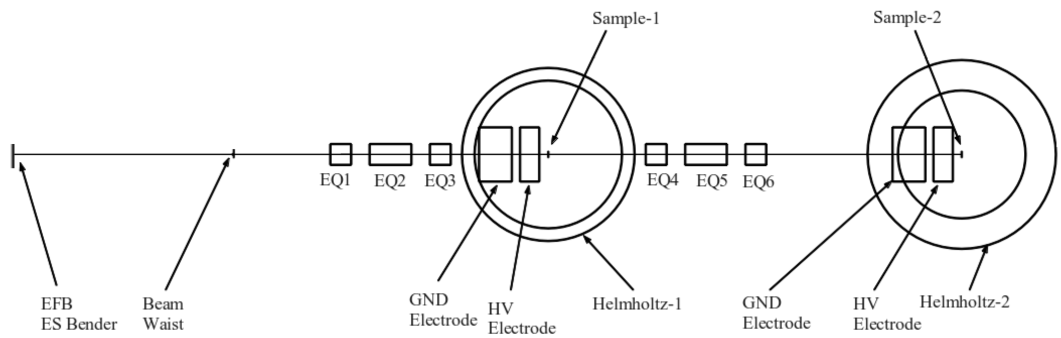

Figure 16: Schematic view of the proposed β-NQR beamline.

5.4 Trajectory calculation

Initially the two electrostatic quadrupole triplets were optimized for stigmatic point-to-parallel-to-point imaging of beam spot from the location of beam waist to sample location by using the code COSY INFINITY and TRANSOPTR. Further the triplets were optimized using the code GPT to maintain a small 2 mm [2 rms] radius beam spot in the presence of the large transverse magnetic field which breaks the axial symmetry. Simulations were performed by tracking the particle ensembles through the beamline. The basic beam parameters used in this simulation are shown in Table 2. The initial phase-space distribution used in this simulation is shown in Fig. 15. The two quadrupole triplets were tuned together in such a way that a point-to-parallel-to-point focusing on sample-2 is achieved.

Beam transport simulations were performed by tracking the particle through the beamline with and without an applied magnetic field. In the case of beam transport through an applied magnetic field of 2000 G the beam spot is positioned on the sample by optimizing the potential of the decelerator electrodes A and C (see Fig. 4). Different potential on the electrodes introduces a quadrupole effect, which is counteracted by tuning the upstream quadrupoles to obtain a round beam on sample-2. The simulated spatial profile for a 28 keV 8Li$^+$ ion beam at the location of sample-2 at 2000 G is shown in see Fig. 20. Calculated trajectories up to sample position 2 are shown in Fig. 18 & 19. The beam parameters at the location of sample-2 are given Table 3 and the corresponding optical settings are shown in Table 4.

In the second case the transport simulation is performed by tracking the particle through the beamline without an applied magnetic field [0 G]. It should be noted that the beamline differs from the initial beamline design to accommodate the heat shielding between the sample and rest of the beamline. Because of this constraint the position of the reference trajectory is fixed irrespective of an applied magnetic field. For an example the vertical deflection due to an external applied magnetic field of 2000 G is around 21 mm at the location of 2.144 m downstream to the bender [ILE2A:B3]. In the case of without an external magnetic field [0 G] two vertical electrostatic steerers are used to achieve a similar vertical deflection [21 mm at Z =2.144 m] as in the case of an applied magnetic field [2000 G]. The beam transport through the aperture of the heat shield is optimized by using these vertical steerers [YCB3 & YCB4]. This is an advantage for the cryostat, i.e., sample does not see any thermal radiation. The additional focusing due to the steerer is compensated by curving the electrode as shown in Fig. 11. Fig. 25 shows the phase-space distributions for without an external magnetic field. Calculated trajectories up to sample-2 are shown in Fig. 23 & 24 and the corresponding optical settings are shown in Table 10.

Also the transport calculations are performed for the sample-1 with an external magnetic field [220 G] and without an external magnetic field [0 G]. The results of phase-space distributions are presented in Figs. 28 & 32 and the corresponding optical settings are tabled in Table 12 & Table 16 respectively.

Detailed beamline components of our beam optics design and its location in the proposed β-NQR beamline are given in Table 17.

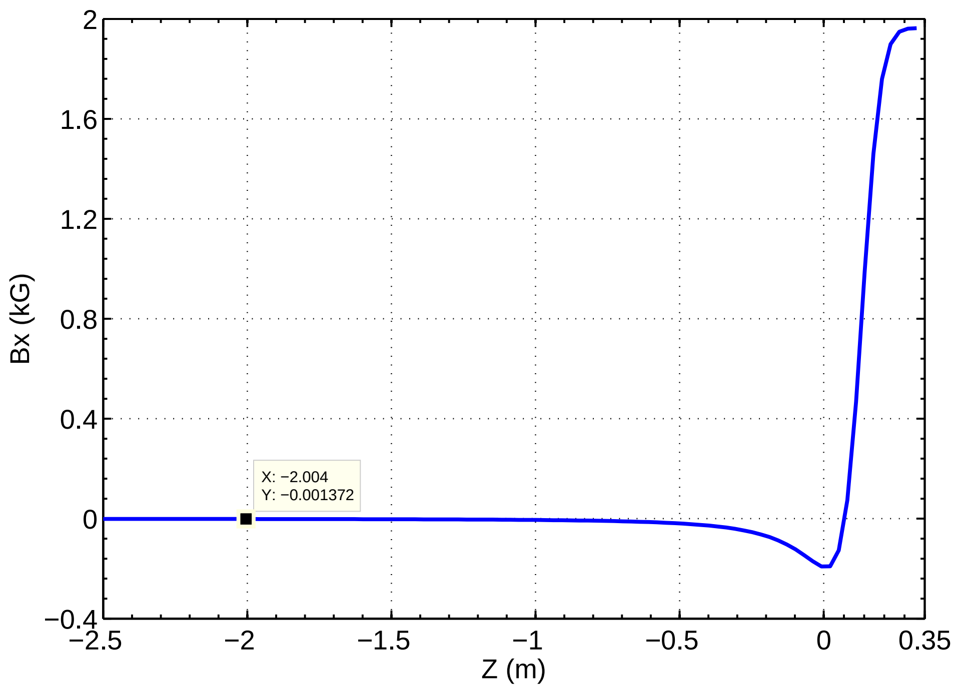

Figure 17: Calculated magnetic field along the beam axis for the proposed Helmholtz coil. Sample-2 location at z = 0.322 m.

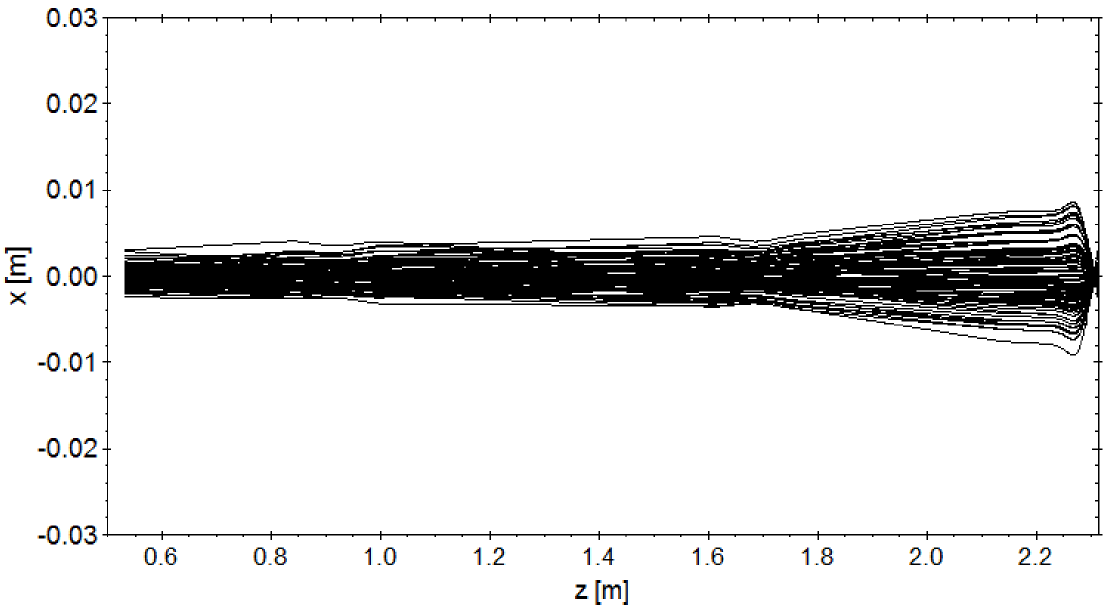

Figure 18: Calculated ion trajectories (100 particles) of 28 keV 8Li+ beam in ZX-plane at 2000 G [Sample-2]. For the optical settings see Table 4.

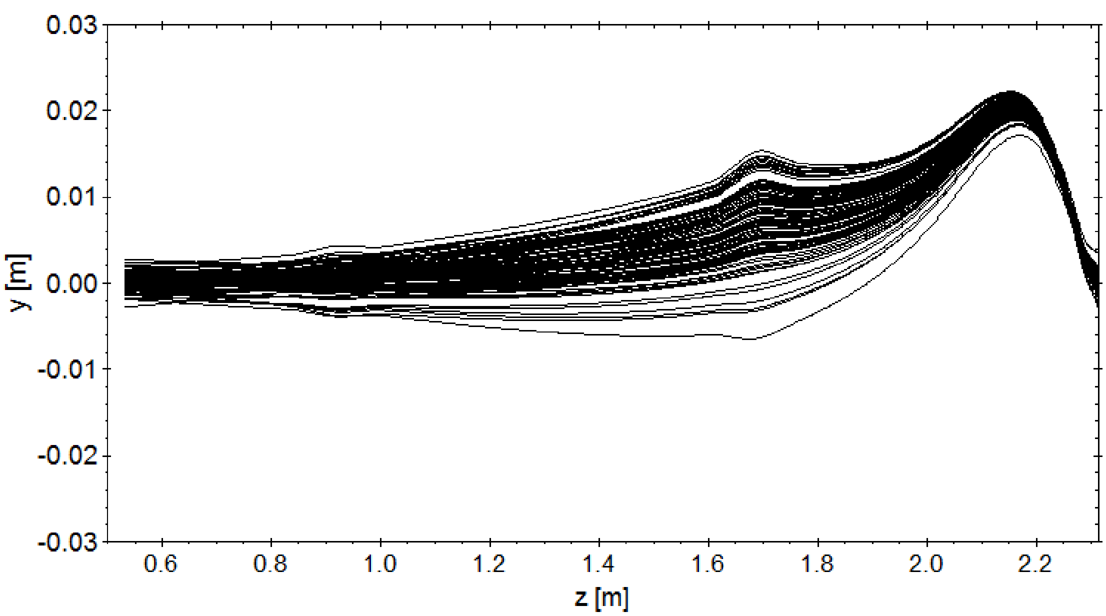

Figure 19: Calculated ion trajectories (100 particles) of 28 keV 8Li+ beam in ZY-plane at 2000 G [Sample-2]. For the optical settings see Table 4.

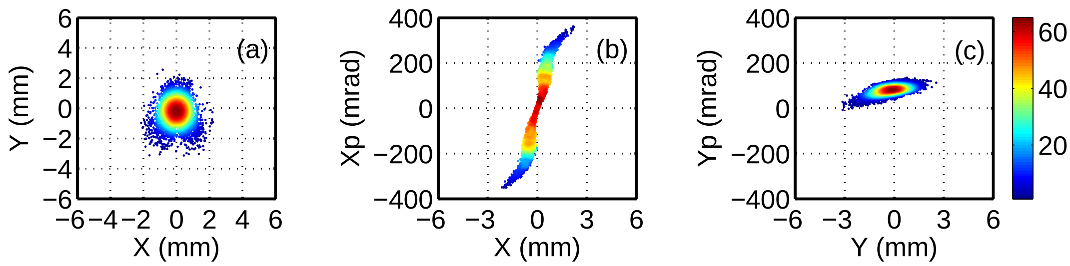

Figure 20: Calculated spatial profile (a), horizontal (b) and vertical (c) phase planes of 4 keV $8Li^+$ beam (10000 particles) at the location of sample-2 with 2000 G Helmholtz field strength. For the beam parameters and optical settings see Table 3 and 4, respectively.

Beam	$8Li^+$
Initial beam energy	28 keV
Beam energy on the sample-2	4 keV
Magnetic field at sample-2	2000 G
X-half width (2 rms)	1.4 mm
Y-half width (2 rms)	1.7 mm
X-emittance (4 rms)	140.0 μm
Y-emittance (4 rms)	37.4 μm
Transmission	98 %

Table 3: Basic beam parameters of 4 keV $8Li^+$ beam at the location of sample-2 with 2000 G Helmholtz field strength.

Beam	$8Li^+$
Initial beam energy	28 keV
Beam energy on the sample-2	4 keV
Magnetic field at sample-2	2000 G
ILE2A1:EQ1	2.794 kV
ILE2A1:EQ2	-1.806 kV
ILE2A1:EQ3	2.794 kV
ILE2A1:EQ4	1.948 kV
ILE2A1:EQ5	-1.932 kV
ILE2A1:EQ6	0.538 kV
ILE2A1:HV2A	14.8 kV
ILE2A1:HV2B	24.0 kV
ILE2A1:HV2C	25.0 kV
ILE2A1:HV2D	24.0 kV
ILE2A1:HH2	2000 G

Table 4: Optimized optical settings for 4 keV $8Li^+$ beam at sample-2 position with 2000 G Helmholtz field strength.

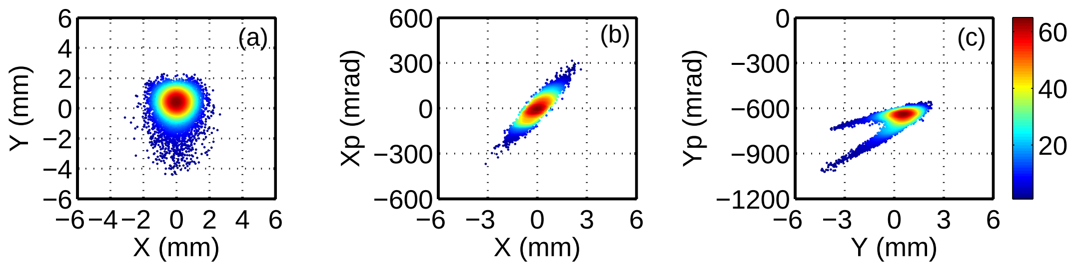

Figure 21: Calculated spatial profile (a), horizontal (b) and vertical (c) phase planes of 1 keV $8Li^+$ beam (10000 particles) at the location of sample-2 with 2000 G Helmholtz field strength. For the beam parameters and optical settings see Table 5 and 6, respectively.

Beam	$8Li^+$
Initial beam energy	28 keV
Beam energy on the sample-2	1 keV
Magnetic field at sample-2	2000 G
X-half width (2 rms)	1.4 mm
Y-half width (2 rms)	1.9 mm
X-emittance (4 rms)	81.1 μm
Y-emittance (4 rms)	183.0 μm
Transmission	99.5 %

Table 5: Basic beam parameters of 1 keV $8Li^+$ beam at the location of sample-2 with 2000 G Helmholtz field strength.

Beam	$8Li^+$
Initial beam energy	28 keV
Beam energy on the sample-2	1 keV
Magnetic field at sample-2	2000 G
ILE2A1:EQ1	2.310 kV
ILE2A1:EQ2	-2.297 kV
ILE2A1:EQ3	2.310 kV
ILE2A1:EQ4	2.126 kV
ILE2A1:EQ5	-2.868 kV
ILE2A1:EQ6	4.000 kV
ILE2A1:YCB4 steerer	1.100 kV
ILE2A1:HV2A	22.0 kV
ILE2A1:HV2B	27.0 kV
ILE2A1:HV2C	25.3 kV
ILE2A1:HV2D	27.0 kV
ILE2A1:HH2	2000 G

Table 6: Optimized optical settings for 1 keV $8Li^+$ beam at sample-2 position with 2000 G Helmholtz field strength.

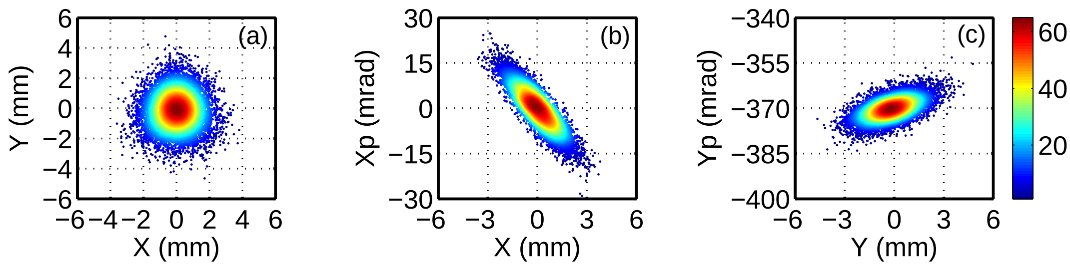

Figure 22: Calculated spatial profile (a), horizontal (b) and vertical (c) phase planes of 28 keV $8Li^+$ beam (10000 particles) at the location of sample-2 with 2000 G Helmholtz field strength. For the beam parameters and optical settings see Table 7 and 8, respectively.

Beam	$8Li^+$
Initial beam energy	28 keV
Beam energy on the sample-2	28 keV
Magnetic field at sample-2	2000 G
X-half width (2 rms)	2.0 mm
Y-half width (2 rms)	2.2 mm
X-emittance (4 rms)	13.0 μm
Y-emittance (4 rms)	13.1 μm
Transmission	100 %

Table 7: Basic beam parameters of 28 keV $8Li^+$ beam at the location of sample-2 with 2000 G Helmholtz field strength.

Beam	$8Li^+$
Initial beam energy	28 keV
Beam energy on the sample-2	28 keV
Magnetic field at sample-2	2000 G
ILE2A1:EQ1	2.271 kV
ILE2A1:EQ2	-2.274 kV
ILE2A1:EQ3	2.271 kV
ILE2A1:EQ4	2.113 kV
ILE2A1:EQ5	-2.839 kV
ILE2A1:EQ6	3.677 kV
ILE2A1:YCB4 steerer	1.100 kV
ILE2A1:HV2A	0.0 kV
ILE2A1:HV2B	0.0 kV
ILE2A1:HV2C	0.0 kV
ILE2A1:HV2D	0.0 kV
ILE2A1:HH2	2000 G

Table 8: Optimized optical settings for 28 keV $8Li^+$ beam at sample-2 position with 2000 G Helmholtz field strength.

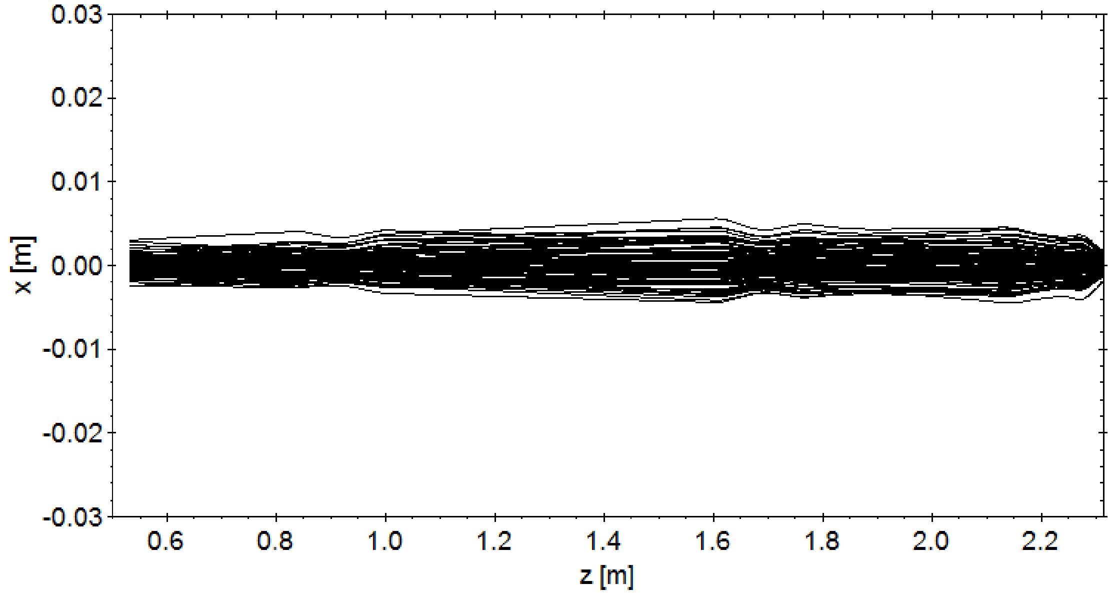

Figure 23: Calculated ion trajectories (100 particles) of 28 keV 8Li+ beam in ZX-plane at 0 G [Sample-2]. For the optical settings see Table 10.

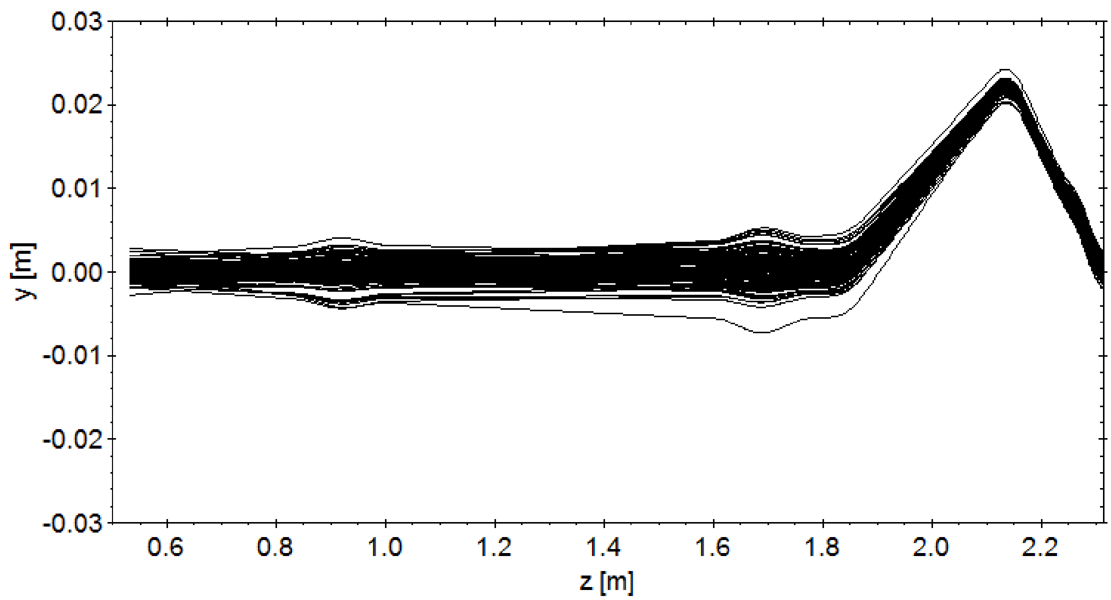

Figure 24: Calculated ion trajectories (100 particles) of 28 keV 8Li+ beam in ZY-plane at 0 G [Sample-2]. For the optical settings see Table 10.

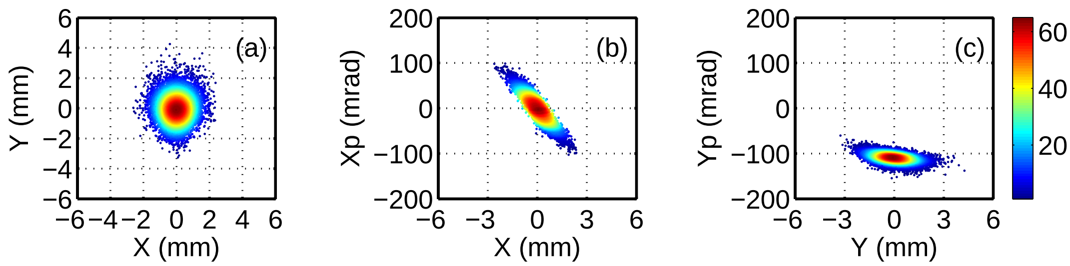

Figure 25: Calculated spatial profile (a), horizontal (b) and vertical (c) phase planes of 4 keV 8Li$^+$ beam (10000 particles) at the location of sample-2 at 0 G. For the beam parameters and optical settings see Table 9 and 10, respectively.

Beam	8Li$^+$
Initial beam energy	28 keV
Beam energy on the sample-2	4 keV
Magnetic field at sample-2	0 G
X-half width (2 rms)	1.3 mm
Y-half width (2 rms)	1.7 mm
X-emittance (4 rms)	32.8 μm
Y-emittance (4 rms)	33.2 μm
Transmission	100 %

Table 9: Basic beam parameters of 4 keV 8Li$^+$ beam at the location of sample-2 with 0 G Helmholtz field strength.

Beam	$8Li^+$
Initial beam energy	28 keV
Beam energy on the sample-2	4 keV
Magnetic field at sample-2	0 G
ILE2A1:EQ1	2.631 kV
ILE2A1:EQ2	-2.576 kV
ILE2A1:EQ3	2.631 kV
ILE2A1:EQ4	3.098 kV
ILE2A1:EQ5	-2.775 kV
ILE2A1:EQ6	3.098 kV
ILE2A1:YCB3 Steerer	4.20 kV
ILE2A1:YCB4 Steerer	3.43 kV
ILE2A1:HV2A	22.9 kV
ILE2A1:HV2B	24.0 kV
ILE2A1:HV2C	26.3 kV
ILE2A1:HV2D	24.0 kV
ILE2A1:HH2	0 G

Table 10: Optimized optical settings for 4 keV $8Li^+$ beam at sample-2 position with 0 G Helmholtz field strength.

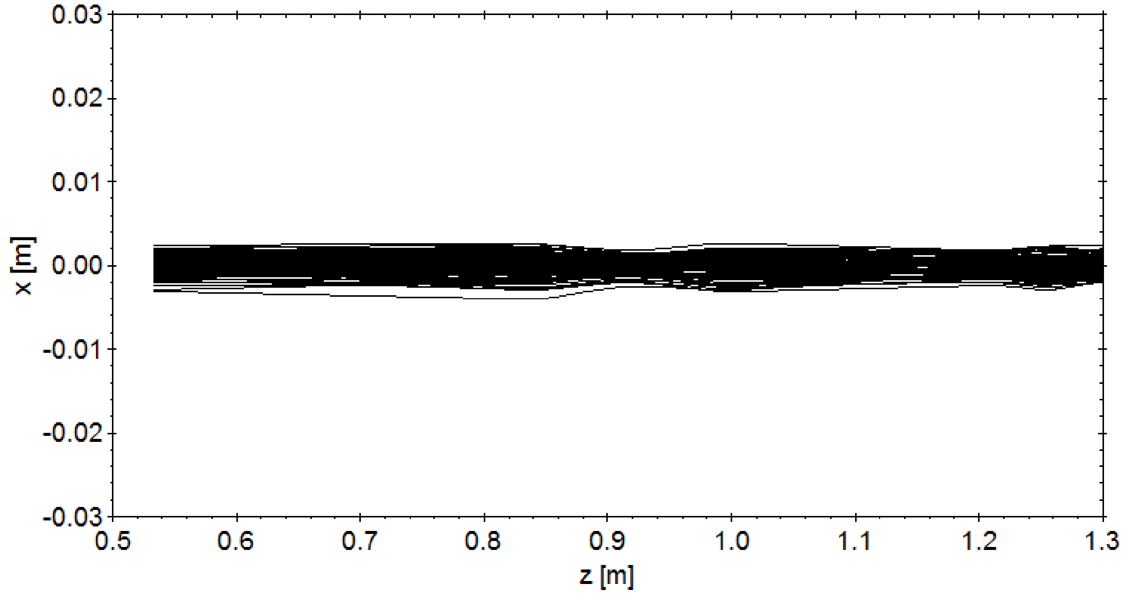

Figure 26: Calculated ion trajectories (100 particles) of 28 keV 8Li+ beam in ZX-plane at 220 G [Sample-1]. For the optical settings see Table 12.

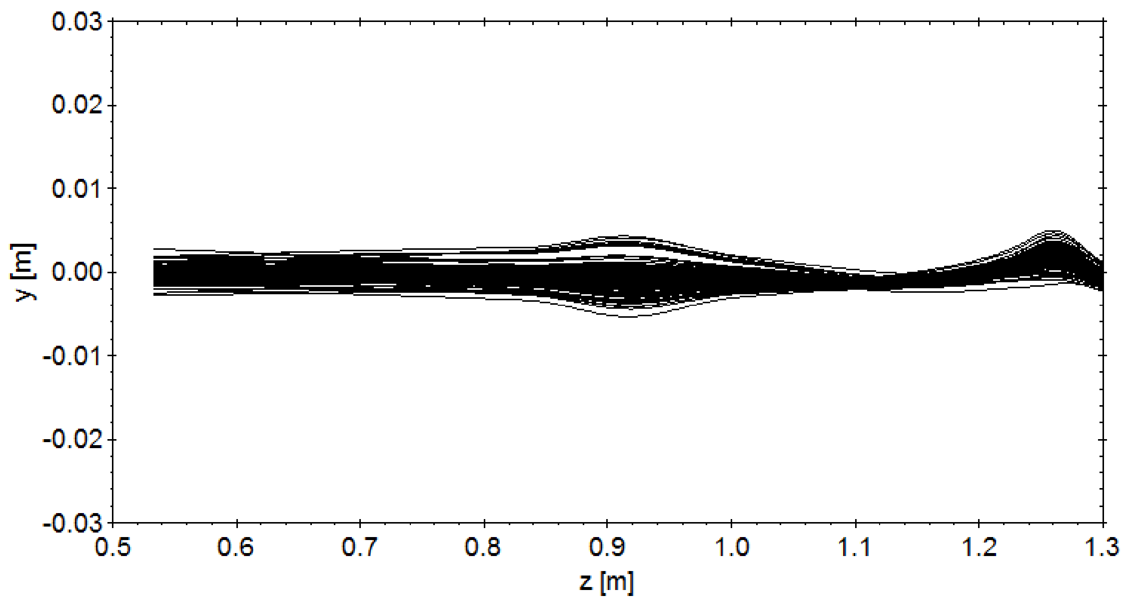

Figure 27: Calculated ion trajectories (100 particles) of 28 keV 8Li+ beam in ZY-plane at 220 G [Sample-1]. For the optical settings see Table 12.

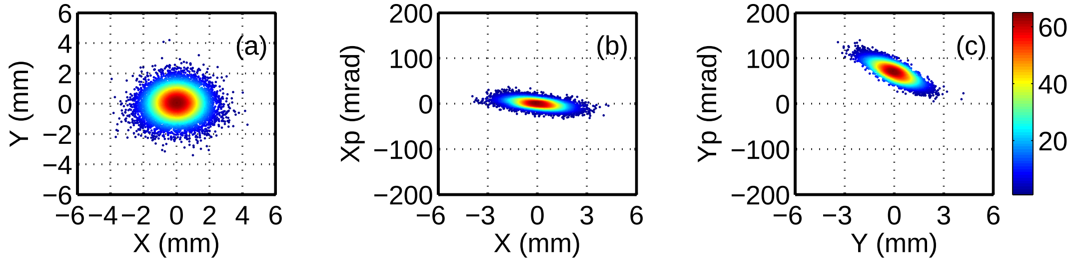

Figure 28: Calculated spatial profile (a), horizontal (b) and vertical (c) phase planes of 4 keV 8Li$^+$ beam (10000 particles) at the location of sample-1 with 220 G Helmholtz field strength.

Beam	8Li$^+$
Initial beam energy	28 keV
Beam energy on the sample-1	4 keV
Magnetic field at sample-1	220 G
X-half width (2 rms)	2.0 mm
Y-half width (2 rms)	1.6 mm
X-emittance (4 rms)	32.6 μm
Y-emittance (4 rms)	32.8 μm
Transmission	100 %

Table 11: Basic beam parameters of 4 keV 8Li$^+$ beam at the location of sample-1 with 220 G Helmholtz field strength.

Beam	$8Li^+$
Initial beam energy	28 keV
Beam energy on the sample-1	4 keV
Magnetic field at sample-1	220 G
ILE2A1:EQ1	4.346 kV
ILE2A1:EQ2	-4.224 kV
ILE2A1:EQ3	4.346 kV
ILE2A1:HV1A	24.0 kV
ILE2A1:HV1B	24.0 kV
ILE2A1:HV1C	25.9 kV
ILE2A1:HV1D	24.0 kV
ILE2A1:HH1	220 G

Table 12: Optimized optical settings for 4 keV $8Li^+$ beam at sample-1 position with 220 G Helmholtz field strength.

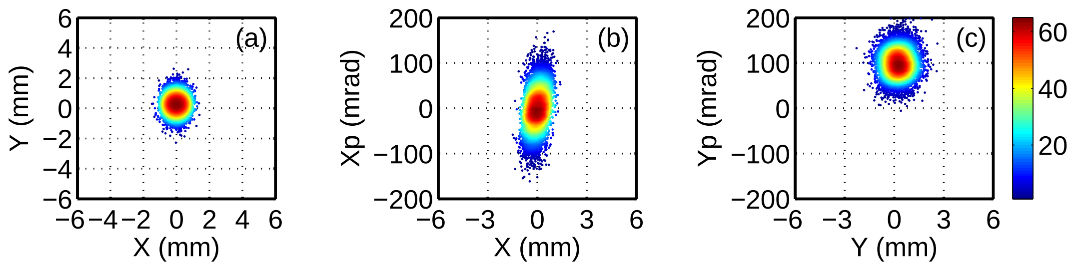

Figure 29: Calculated spatial profile (a), horizontal (b) and vertical (c) phase planes of 1 keV $8Li^{+}$ beam (10000 particles) at the location of sample-1 with 220 G Helmholtz field strength.

Beam	$8Li^{+}$
Initial beam energy	28 keV
Beam energy on the sample-1	1 keV
Magnetic field at sample-1	220 G
X-half width (2 rms)	0.74 mm
Y-half width (2 rms)	1.1 mm
X-emittance (4 rms)	62.1 μm
Y-emittance (4 rms)	65.0 μm
Transmission	100 %

Table 13: Basic beam parameters of 1 keV $8Li^{+}$ beam at the location of sample-1 with 220 G Helmholtz field strength.

Beam	$8Li^+$
Initial beam energy	28 keV
Beam energy on the sample-1	1 keV
Magnetic field at sample-1	220 G
ILE2A1:EQ1	5.070 kV
ILE2A1:EQ2	-4.224 kV
ILE2A1:EQ3	5.070 kV
ILE2A1:HV1A	25.6 kV
ILE2A1:HV1B	27.0 kV
ILE2A1:HV1C	27.0 kV
ILE2A1:HV1D	27.0 kV
ILE2A1:HH1	220 G

Table 14: Optimized optical settings for 1 keV $8Li^+$ beam at sample-1 position with 220 G Helmholtz field strength.

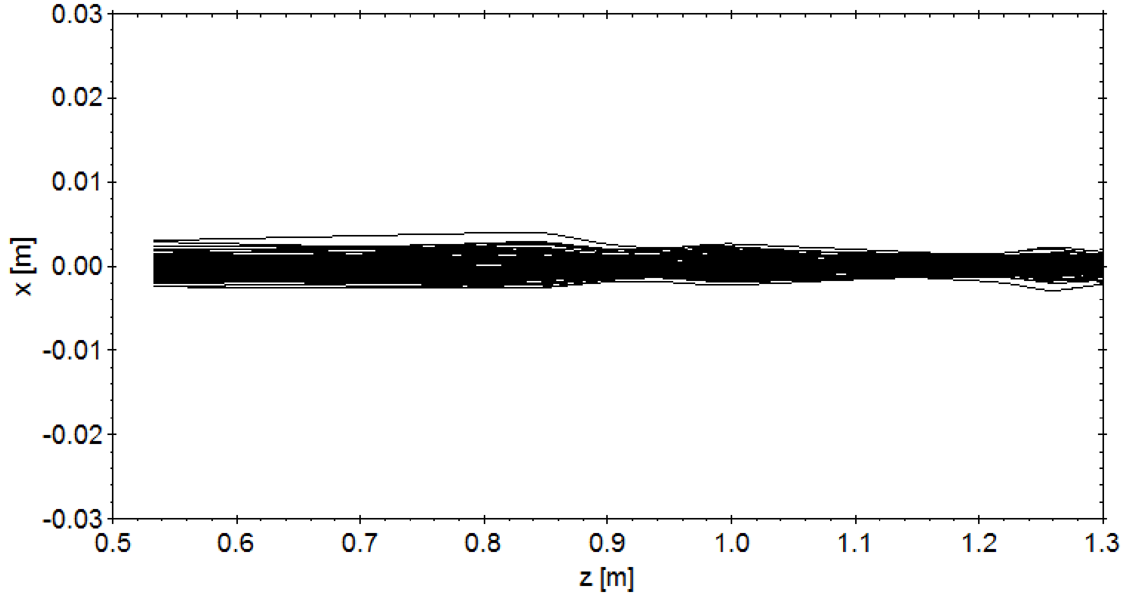

Figure 30: Calculated ion trajectories (100 particles) of 28 keV 8Li+ beam in ZX-plane at 0 G [Sample-1]. For the optical settings see Table 16.

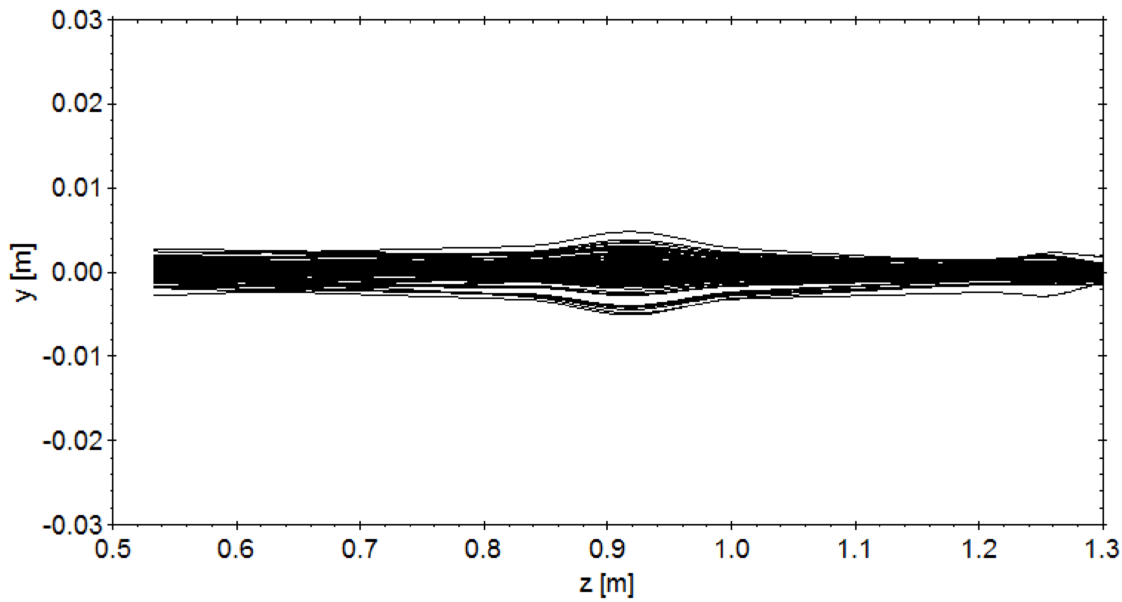

Figure 31: Calculated ion trajectories (100 particles) of 28 keV 8Li+ beam in ZY-plane at 0 G [Sample-1]. For the optical settings see Table 16.

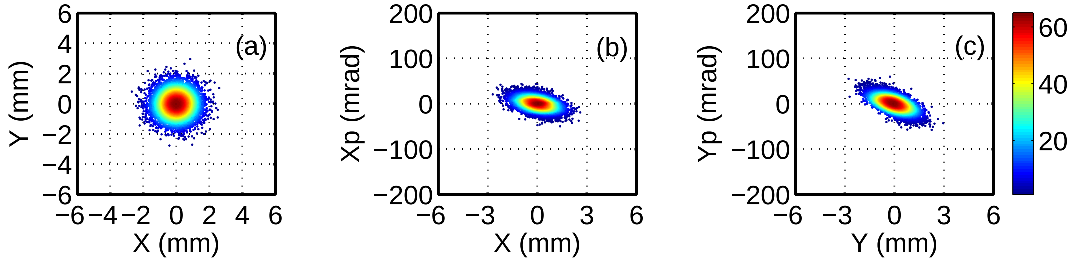

Figure 32: Calculated spatial profile (a), horizontal (b) and vertical (c) phase planes of 4 keV $8Li^{+}$ beam (10000 particles) at the location of sample-1 with 0 G Helmholtz field strength.

Beam	$8Li^{+}$
Initial beam energy	28 keV
Beam energy on the sample-1	4 keV
Magnetic field at sample-1	0 G
X-half width (2 rms)	1.37 mm
Y-half width (2 rms)	1.38 mm
X-emittance (4 rms)	31.3 μm
Y-emittance (4 rms)	31.9 μm
Transmission	100 %

Table 15: Basic beam parameters of 4 keV $8Li^{+}$ beam at the location of sample-1 with 0 G Helmholtz field strength.

Beam	$8Li^{+}$
Initial beam energy	28 keV
Beam energy on the sample-1	4 keV
Magnetic field at sample-1	0 G
ILE2A1:EQ1	4.636 kV
ILE2A1:EQ2	-3.931 kV
ILE2A1:EQ3	4.636 kV
ILE2A1:HV1A	24.0 kV
ILE2A1:HV1B	24.0 kV
ILE2A1:HV1C	24.0 kV
ILE2A1:HV1D	24.0 kV
ILE2A1:HH1	0 G

Table 16: Optimized optical settings for 4 keV $8Li^{+}$ beam at sample-1 position with 0 G Helmholtz field strength.

6 Diagnostics

In the current β-NQR apparatus, focusing and steering of the beam on the sample are diagnosed by replacing the sample with a scintillator and imaging with a CCD camera. The new spectrometer would have a similar system. The spectrometer will be UHV compatible in order to avoid a buildup of residual gases on the surface of the sample. Differential pumping is required to reduce the pressure from 10^{-7} Torr upstream of the spectrometer to 10^{-10} Torr in the main chamber.

Components	Distance [mm]	Length [mm]	Radius [mm]	Comments
ILE2A:B3	0.00	–	–	EBEND-EFB
ILE2A1:YCB1 Steerer	340.00	–	–	Ref:Existing ILE2A1 UHV steerer
ILE2A1:XCB1 Steerer	390.80	–	–	Ref:Existing ILE2A1 UHV steerer
Collimator/FC1/RPM	533.40	0.00	0.00	Location of the beam waist
EQ1	844.53	25.40	25.40	Ref:ISAC-LEBT-UHV EQ
EQ2	918.69	50.80	25.40	Ref:ISAC-LEBT-UHV EQ
EQ3	992.85	25.40	25.40	Ref:ISAC-LEBT-UHV EQ
YCB2 Steerer	1079.45	–	–	Ref:ISAC
XCB2 Steerer	1136.65	–	–	Ref:ISAC-LEBT
GND1	1197.70	50.80	–	Ref:Fig. 5
HV1	1257.80	25.40	–	Ref:Fig. 4
HH1	1292.50	–	–	[3]Ref:Fig. 1
Focus at sample-1 [MCP]	1292.50	–	–	For 220 G
FC2	1470.0	–	–	Ref:ISAC-LEBT
EQ4	1615.11	25.40	25.4	Ref:ISAC-LEBT-UHV EQ
EQ5	1689.27	50.80	25.4	Ref:ISAC-LEBT-UHV EQ
EQ6	1763.43	25.40	25.4	Ref:ISAC-LEBT-UHV EQ
YCB3 Steerer	1850.03	–	–	Ref:ISAC-LEBT [2 inch full gap]
XCB3 Steerer	1907.23	–	–	Ref:ISAC-LEBT
FC3	2055.10	–	–	Ref:ISAC-LEBT
YCB4 Steerer	2144.00	–	–	Ref:Fig. 12
GND2	2221.12	50.80	–	Ref:Fig. 5
HV2	2279.30	25.40	–	Ref:Fig. 4
HH2	2314.00	–	–	Ref:Fig. 6 & 7
Focus at sample-2 [MCP]	2314.00	–	–	For 2000 G
FC4	2492.0	–	–	Ref:ISAC-LEBT

Table 17: Beamline components and its center position in the proposed β-NQR beamline.

6.1 Constraints

- Calculated beam envelope must fit into the beamline components with a minimum clearance of 6 mm.
- A protective plate (grounded electrode) is required for the quadrupoles in the second triplet (in the section of sample-2).
- All the electrodes must be UHV and HV compatible.
- A minimum gap of 20 mm is required between decelerator (HV electrode) and the vacuum chamber.

7 Summary

In order to minimize the thermal radiation the beamline optics has been designed to accommodate the heat shield between the sample-2 and rest of the beamline. The proposed beamline will accommodate two samples called sample-1 and sample-2 at two different magnetic field regime, i.e. sample-1 will be at a maximum field of 220 G and sample-2 will be at a maximum field of 2000 G. The beamline layout, beam optics, the corresponding beamline components and its location are presented.

References

[1] R.F. Kiefl, et.al., *Low-energy spin-polarized radioactive beams as a nano-scale probe of matter*, Physica B: Condensed Matter, Volume 326, February 2003, Pages 189195.

[2] L. Merminga, et.al., *A High Magnetic Field Spectrometer as a Surface Probe of Nb Superconductors used in RF Cavities*, Internal report, TRIUMF, Oct., 2013.

[3] George S. Clark, *Concept design of a Helmholtz coil pair for the ISAC polarimeter station*, TRI-DN-01-11, Internal report, TRIUMF, May, 2001.

[4] G. D. Morris, *ISAC polarimeter station*, TRI-DN-01-10, Internal report, TRIUMF, April, 2001.

[5] C.D.P. Levy, et.al., *A polarized beam project at ISAC*, Nuclear Physics A, 701, (2002), 253c–258c.

[6] Thomas Prokscha, *A muon beam project at PSI*, Private communication.

[7] S. Saminathan, *Simulation and measurement of ion beam transport for β-NQR beamline*, TRI-BN-13-06, Internal report, TRIUMF, October, 2013.